Oxidative Substitution of Carbonyl Groups by Halogen or RS• on the Cubane Cluster $Cp^{Et}{}_2Mo_2Co_2S_4(CO)_2$: Preparation of 58-VSE Electron-Deficient Clusters as Models for an Organometallic Desulfurization Material

M. Adnan Mansour, M. David Curtis,* and Jeff W. Kampf

Department of Chemistry, Willard H. Dow Laboratory, The University of Michigan, Ann Arbor, Michigan 48109-1055

Received February 7, 1997[⊗]

The heterobimetallic sulfido cluster $Cp^{Et}{}_2Mo_2Co_2S_4(CO)_2$ was oxidized to give a series of 58-VSE (valence shell electron) electron-deficient clusters of the type $Cp^{Et}{}_2Mo_2Co_2S_4(X)_2$ (X = I, Br, Cl, SPh). These clusters have been structurally characterized by X-ray diffraction. Their magnetic behavior was investigated to reveal complex spin equilibria for the halide-substituted clusters (X = I, Br, Cl) and simple paramagnetism for the thiolate substituted cluster (X = SPh). In an attempted catalytic reaction, $Cp^{Et}{}_2Mo_2Co_2S_4(CO)_2$ reacted with excess benzene thiol under 1000 psi of CO at 150 °C to give phenylthiobenzoate, PhS(CO)-Ph, and PhSSPh in excess of the stoichiometric amounts.

Introduction

The hydrodesulfurization (HDS) of fossil fuels represents a process which is practiced globally on an immense scale.[1] Molybdenum sulfur compounds are important in the desulfurization of organic sulfur compounds[2] and in the HDS catalytic reaction.[3] The commercial HDS catalyst generally consists of a MoS_2 phase promoted by the addition of Co or Ni and is supported on high surface area alumina.[3,4] Thus, the preparation of Mo/S compounds as models for the commercial catalyst has been extensive.[2,5] The reactions of Mo/Co/S containing clusters, principally $Cp'_2Mo_2Co_2S_3(CO)_4$, with organic sulfur compounds have been used to model the reactions which occur with the commercial Co/Mo/S HDS catalyst.[6] This cluster has been shown to mediate S atom abstraction from organic sulfur compounds with the concomitant formation of the cubane cluster $Cp'_2Mo_2Co_2S_4(CO)_2$ and the desulfurized organic hydrocarbon.[6,7] A detailed kinetic study by Druker and Curtis[7] has shown that the rate-determining step in the desulfurization of thiols is the coordination of the thiol to the $Cp'_2Mo_2Co_2S_3(CO)_4$ cluster and that the sulfur is removed by a C−S bond homolysis reaction.

In a recent communication, we reported that the cubane cluster $Cp^{Et}{}_2Mo_2Co_2S_4(CO)_2$ (**1**), where $Cp^{Et} = EtMe_4C_5$, will react with good sulfur donors, *i.e.*, thiiranes and thietanes.[8] In these reactions, the desulfurization of the organic sulfur compound gave the corresponding hydrocarbon and the organometallic product was a black, insoluble solid for which the proposed structure consisted, at least partially, of $Cp^{Et}{}_2Mo_2Co_2S_4$ cubes linked together with sulfide bridges (**2**). Replacement of carbonyl groups in **1** by sulfide bridges in **2** represents an oxidization of the cubane core. Since the organometallic product obtained in the desulfurization reactions was an insoluble, intractable solid, a study of oxidative substitution reactions of **1** as models for the proposed sulfur-bridged clusters was undertaken. This paper describes the preparation, structures, and magnetic behavior of the oxidized clusters. This investigation also revealed that **1** will desulfurize PhSH and, under appropriate conditions, facilitate a catalytic sulfur abstraction reaction.

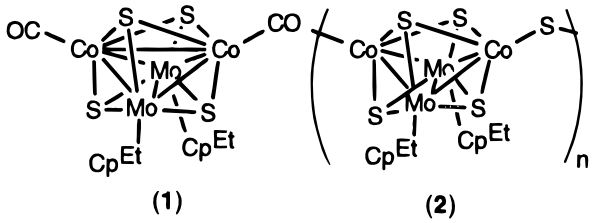

(1) **(2)**

Experimental Section

All manipulations and reactions were carried out under a dinitrogen atmosphere using standard Schlenk line techniques or in an inert atmosphere glove box. Reagent grade solvents were dried and distilled prior to use: toluene, tetrahydrofuran (THF), and diethyl ether from Na/benzophenone; dichloromethane and hexane from CaH_2; isobutyl alcohol (^{i}BuOH) from Mg/I_2. $Cp^{Et}{}_2Mo_2Co_2S_4(CO)_2$ was prepared according to

[⊗] Abstract published in *Advance ACS Abstracts,* July 1, 1997.

(1) Angelici, R. J. In *Encyclopedia of Inorganic Chemistry*; King, R. B., Ed.; John Wiley and Sons: New York, 1994; Vol. 3; pp 1433−1443.
(2) (a) Luh, T.-Y.; Ni, Z.-J. *Synthesis* **1990**, 89. (b) Dubois, M. R. *Chem. Rev.* **1989**, *89* (1), 1. (c) Lopez, L.; Godzeila, G.; Dubois, M. R. *Organometallics* **1991**, *10*, 2660.
(3) Chianelli, R. R.; Daage, M.; Ledoux, M. J. *Adv. Catal.* **1994**, *40*, 177.
(4) (a) Prins, R.; de Beer, V. H. J.; Somorjai, G. A. *Catal. Rev.-Sci. Eng.* **1989**, *31*, 1. (b) Alstrup, I.; Chorkendorff, I.; Candia, R.; Clausen, B. S.; Topsoe, H. *J. Catal.* **1982**, *77*, 397.
(5) For example: (a) Chu, T.-W. C.; Lo, F. Y. K.; Dahl, L. F. *J. Am. Chem. Soc.* **1982**, *104*, 3409. (b) Armstrong, W. H.; Mascharak, P. K.; Holm, R. H. *Inorg. Chem.* **1982**, *21*, 1701. (c) Brunner, H.; Kauermann, H.; Wachter, J. *Angew. Chem., Int. Ed. Engl.* **1983**, *22*, 549. (d) Halbert, T. R.; Cohen, S. A.; Steifel, E. I. *Organometallics* **1985**, *4*, 1689. (e) Li, P.; Curtis, M. D. *Inorg. Chem.* **1990**, *29*, 1242.
(6) (a) Riaz, U.; Curnow, O. J.; Curtis, M. D. *J. Am. Chem. Soc.* **1994**, *116*, 4357. (b) Curtis, M. D. *Appl. Organomet. Chem.* **1992**, *6*, 429.
(7) (a) Druker, S. H.; Curtis, M. D. *J. Am. Chem. Soc.* **1995**, *117*, 6366. (b) Curtis, M. D.; Druker, S. H. *J. Am. Chem. Soc.* **1997**, *119*, 1027.
(8) Mansour, M. A.; Curtis, M. D.; Kampf, J. W. *Organometallics* **1995**, *14*, 5460.

S0276-7333(97)00093-9 CCC: $14.00

the published procedure.[9] All other reagents were used as purchased from Aldrich Chemical Company or Fisher Chemical, Inc.

^{1}H NMR spectra were collected on a Bruker AM-360 or AM-300 spectrometer and referenced to the residual proton solvent reference. FT-IR spectra were collected on a Nicolet 5-DXB spectrometer, and the spectra were corrected for background and solvent effects. Mass spectra were collected on a VG 70-250-S high-resolution spectrometer. The molecular ion peaks reported correspond to the most intense peak in a polyisotopic pattern. GC-MS analyses were obtained on a capillary column interfaced with a Finnegan model 4500 mass spectrometer. Elemental analyses were performed by the Microanalysis Laboratory, The University of Michigan.

Preparation of $Cp^{Et}_2Mo_2Co_2S_4I_2$ (3) from the Reaction of $Cp^{Et}_2Mo_2Co_2S_4(CO)_2$ (1) with I_2. A 100 mL Schlenk flask was charged with $Cp^{Et}_2Mo_2Co_2S_4(CO)_2$ (0.052 g, 0.0656 mmol). A solution of I_2 (0.017 g, 0.0669 mmol) in toluene (30 mL) was added *via* cannula, and the reaction mixture was allowed to stir for 30 min. The yellow-brown solution was then filtered through a 3 cm plug of Celite, which was washed with toluene until the washings were colorless. The filtrate was stripped of solvent, and the product was dried *in vacuo*. Recrystallization from CH_2Cl_2/^{i}BuOH gave 0.054 g (83% yield) of black rectangular crystal plates. ^{1}H NMR ($CDCl_3$): δ 3.07 (br s, 6H, CpCH_3), 2.88 (br s, 6H, CpCH_3), 2.01 (br s, 3H, CpCH$_2CH_3$), 1.88 (br s, 2H, CpCH_2CH$_3$). Anal. Calcd for $Cp^{Et}_2Mo_2Co_2S_4I_2 \cdot {}^1/_2CH_2Cl_2$: C, 26.17; H, 3.42. Found: C, 26.05; H, 3.18. High-resolution mass spectrum (HRMS), *m*/*z*: calcd, 981.6433; found, 981.6432.

Preparation of $Cp^{Et}_2Mo_2Co_2S_4Br_2$ (4) from 1 and Br_2. A solution of Br_2 (0.30 mL, 0.058 mol) in CH_2Cl_2 (20 mL) was prepared; [Br_2] = 0.29 M. To a solution of $Cp^{Et}_2Mo_2Co_2S_4(CO)_2$ (0.132 g, 0.167 mmol) in CH_2Cl_2 (30 mL), Br_2 (0.60 mL of the 0.29 M solution, 0.17 mmol) was added *via* syringe, and the solution was allowed to stir at room temperature for 15 min. The deep green solution was then filtered through a 3 cm plug of Celite, which was washed with CH_2Cl_2 until the washings were colorless. Recrystallization from CH_2Cl_2/hexane gave 0.101 g (68% yield) of black rectangular crystal plates. ^{1}H NMR ($CDCl_3$): δ 2.90 (br s, 6H, CpCH_3), 2.69 (br s, 6H, CpCH_3), 1.98 (m, 5H, CpCH_2CH_3). Anal. Calcd for $Cp^{Et}_2Mo_2Co_2S_4(Br)_2$: C, 29.48; H, 3.82. Found: C, 29.13; H, 3.70. MS, *m*/*z*: 896 (M^+), 815 ($M^+ - Br$), 735 ($M^+ - 2Br$).

Preparation of $Cp^{Et}_2Mo_2Co_2S_4Cl_2$ (5) from 1 and Cl_2. In a 100 mL Schlenk flask, a solution of $Cp^{Et}_2Mo_2Co_2S_4(CO)_2$ (0.146 g, 0.184 mmol) in CH_2Cl_2 (100 mL) was prepared. Using a gas-tight syringe, Cl_2 (5 mL, 0.223 mmol) was added to the $Cp^{Et}_2Mo_2Co_2S_4(CO)_2$ solution, and the reaction mixture was stirred at room temperature for 2 h. The deep green solution was then filtered through a 2 cm plug of Celite, which was washed with CH_2Cl_2 until the washings were colorless. Recrystallization from CH_2Cl_2/hexane gave 0.071 g (48% yield) of black rectangular crystal plates. ^{1}H NMR ($CDCl_3$): δ 2.77 (br s, 6H, CpCH_3), 2.56 (br s, 6H, CpCH_3), 1.95 (br m, 5H, CpCH_2CH_3). Anal. Calcd for $Cp^{Et}_2Mo_2Co_2S_4(Cl)_2 \cdot CH_2Cl_2$: C, 30.95; H, 4.07. Found: C, 31.80; H, 4.12. MS, *m*/*z*: 808 (M^+), 771 ($M^+ - Cl$), 734 ($M^+ - 2Cl$).

Preparation of $Cp^{Et}_2Mo_2Co_2S_4(SPh)_2$ (6) from 1 and PhSSPh. In a 100 mL Schlenk flask, $Cp^{Et}_2Mo_2Co_2S_4(CO)_2$ (0.059 g, 0.0744 mmol) and PhSSPh (0.018 g, 0.0824 mmol) were dissolved in toluene (30 mL). The solution was heated at reflux for 1 h, at which point no ν_{CO} were observed in the solution IR spectrum. The dark blue solution was filtered, hot, through a 4 cm plug of Celite, which was washed with toluene until the washings were colorless. Recrystallization from toluene/hexane at −18 °C gave 0.041 g (58% yield) of long, black, needle-like crystals. No ^{1}H NMR spectrum was obtained (paramagnetic). Anal. Calcd for $C_{34}H_{44}Mo_2Co_2S_6$ ($Cp^{Et}_2Mo_2Co_2S_4(SPh)_2$): C, 42.77; H, 4.64. Found: C, 42.49; H, 4.55. The material did not maintain its integrity upon ionization for mass spectral analysis.

Preparation of 6 from 1 and PhSH. In a 100 mL Schlenk flask, a solution of **1** (0.079 g, 0.100 mmol) in toluene (30 mL) was prepared. To this yellow-brown solution, PhSH (0.10 mL, 0.974 mmol) was added. A reflux condenser was attached to the flask, and under a blanket of N_2, the reaction mixture was heated at reflux for 2.5 h. The solution had become deep blue in color, and a solution IR spectrum revealed no ν_{CO}. The reaction mixture was stripped of solvent, and the residue was washed with hexane to extract unreacted PhSH. Recrystallization from 1:2.5 toluene/hexane gave $Cp^{Et}_2Mo_2Co_2S_4(SPh)_2$ (**6**). Yield: 0.017 g (17%). Anal. Calcd for $C_{34}H_{44}Mo_2Co_2S_6$: C, 42.77; H, 4.64. Found: C, 41.47; H, 4.63.

Reaction of 6 with H_2/CO. In a glovebag, a 40 mL Parr pressure reactor was charged with **6** (0.070 g, 0.073 mmol) and toluene (10 mL). The vessel was sealed and charged with H_2 (200 psi) and CO (200 psi). The system was heated at 130 °C for 10 h. The reactor was depressurized, and in a glovebag, the contents were transferred to a 100 mL Schlenk flask. A solution IR spectrum revealed ν_{CO} = 1956 and 1973 cm^{-1}. The solvent was removed *in vacuo*, the residual solid was washed with hexane, and this extract was filtered through a plug of Celite. GC/MS analysis revealed the presence of PhSSPh (M^+ = 218) as the only organic product.

Reaction of 1 with PhSH and CO. A 300 mL Parr pressure reactor was charged with **1** (0.095 g, 0.120 mmol), sealed, and purged with N_2 for 30 min. A solution of PhSH (2.0 mL, 19.5 mmol) in toluene (50 mL) was added to the reactor *via* cannula through the liquid extraction port, and the reactor was charged with CO (1000 psi) and heated at 150 °C for 46 h. The vessel was depressurized, and in a glovebag, the contents were transferred to a 100 mL Schlenk flask. The volatiles and solvent were distilled *in vacuo* and analyzed by GC-MS; only PhSH was observed in the GC trace. A cold finger was attached to the flask, and sublimation of organic byproducts was completed. Analysis of the sublimed components (0.086 g) by GC-MS revealed PhSSPh (M^+, 218), 171%, PhS(CO)Ph (M^+, 214), 161%. The yields were based on **1** and were calculated by multiplying the percent composition (determined by GC/MS) by the mass of the sublimed material. The residual organometallic product was recrystallized from 1:5 toluene/hexane at −18 °C to give **6**. Yield: 0.053 g, 57%.

Magnetic Susceptibility Measurements. Magnetic susceptibility measurements were made using a Quantum Design MPMS SQUID magnetometer with an applied field of 1000 G. Magnetizations were measured through a temperature range of 4−300 K. The samples were contained in calibrated gelatin capsules held in the center of a soda straw fixed to the end of the sample rod. The magnetization values of the instrument were calibrated against a standard palladium sample supplied by Quantum Design.

X-ray Structural Analyses. X-ray Data Collection. Black crystals of **3**, **5**, and **6** were sealed in thin-walled capillaries in air. These crystals were mounted on a Syntex $P2_1$m/v diffractometer (**3** and **6**) or transferred to the cold stream on a Siemens R2m/v (**5**) equipped with an LT-2 low-temperature device at 138 K. The unit-cell dimensions were obtained from the least-squares fit of 38 reflections (15.0° ≤ 2θ ≤ 34.5°) (**3**), 26 reflections each for (20.2° ≤ 2θ ≤ 34.3°) (**5**) and (15.0° ≤ 2θ ≤ 30.0°) (**6**). Molecules of **3** and **5** lie on general positions but those of **6** lie on 2-fold rotation axes that pass through the midpoints of the Mo−Mo and Co−Co atom positions. In **3**, the structure contains a dichloromethane solvent molecule placed at $^1/_2$ occupancy. The solvent is disordered on a site of 2-fold symmetry in the lattice. Three standard reflections, monitored every 97 data points for all structures, showed insignificant variations (<2%) for **3** and **5** and a linear decay of ca. 4% for **6**. Empirical absorption corrections based on azimuthal scans (Ψ scans) were applied to the data sets, which were also corrected for Lorentz and polarization effects.

(9) Brunner, H.; Wachter, J. *J. Organomet. Chem.* **1982**, *240*, C41.

Scheme 1

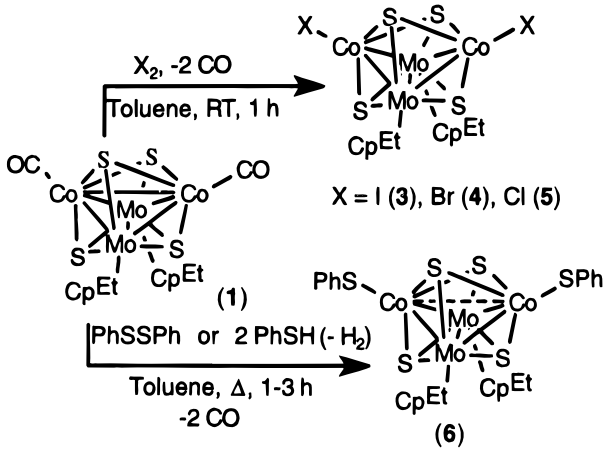

Structure Solution and Refinement. The structures for **3** and **5** were solved by direct methods to locate the metal atoms, whereas **6** was solved by a Patterson map. The remaining non-hydrogen atoms were located through subsequent difference Fourier syntheses. All non-hydrogen atoms were refined with anisotropic thermal parameters, and all hydrogen atoms were fit using the riding model ($d_{C-H} = 0.96$ Å, common U(H)). Refinement was by full-matrix least-squares techniques (**3** and **6**) or full-matrix least-squares techniques based on F^2 (**5**) to minimize the function $\sum w(|F_o| - F_c|)^2$ (**3** and **6**) or $\sum w(|F_o^2 - F_c^2|)^2$ (**5**) with $w = 1/[\sigma^2(F_o) + 0.000\,765(F_o)^2]$ (**3**), $w = 1/[\sigma^2(F_o) + (0.1902P)^2 + 24.58P]$ (**5**) where $P = [\max(F_o^2, 0) + 2F_c^2]/3$, and $w = 1/[\sigma^2(F_o) + 0.000\,389(F_o)^2]$ (**6**). Crystals of **5** were small and weakly diffracting, leading to a large R value. Furthermore, the refinement on F^2 gives an R_w that is defined differently from the usual R_w based on F and is always at least twice the value of the more usual R_w (see footnote to Table 3 for definitions). All calculations were performed on a VAX Station 3500 computer using the Siemens SHELXTL PLUS[10] software package (**3**) or using the SHELXTL PLUS, SHELXL-93[11] software package (**5**).

Results and Discussion

Synthesis. A new series of halide-substituted and thiolate-substituted clusters were prepared by oxidative substitution of CO on the cluster $Cp^{Et}{}_2Mo_2Co_2S_4(CO)_2$ (**1**), as shown in Scheme 1. At room temperature, cluster **1** reacted readily with 1 equiv of I_2 in toluene to give the new cluster $Cp^{Et}{}_2Mo_2Co_2S_4(I)_2$ (**3**) in high isolated yield (83%) subsequent to crystallization from CH_2Cl_2/^{t}BuOH. This species was analytically pure, and the ^{1}H NMR spectrum appeared to be that of a diamagnetic compound with peaks due to the Cp^{Et} ligands at δ 3.07 and 2.88 (Me groups) and 2.01 and 1.88 (Et group). The far-IR spectrum showed a prominent band at 398 cm^{-1}, which is assigned to the (μ_3-S)−M stretching absorption in analogy to other similar thiocubane molecules,[5d,12] and other strong absorptions at 236 and 290 cm^{-1}, which are assigned to the Co−I stretching modes.[13] The solid-state structure of this compound was determined by single-crystal X-ray diffraction and is discussed below.

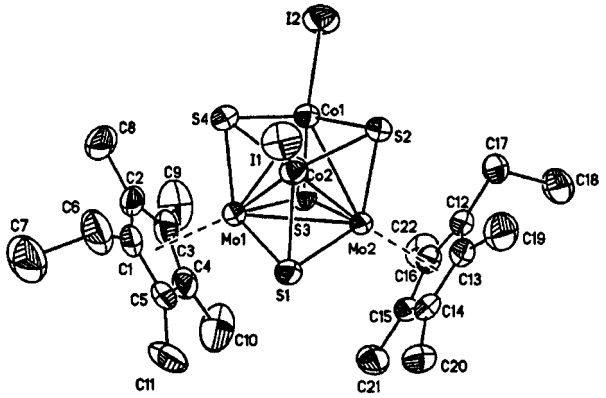

Figure 1. ORTEP plot of $Cp^{Et}{}_2Mo_2Co_2S_4(I)_2$ (**3**) with the atomic numbering scheme. Thermal ellipsoids are drawn at the 50% probability level.

In analogous reactions, cluster **2** reacted with 1 equiv of Br_2 in CH_2Cl_2 or a slight excess of Cl_2 in CH_2Cl_2 at room temperature to give the analytically pure clusters $Cp^{Et}{}_2Mo_2Co_2S_4(Br)_2$ (**4**) and $Cp^{Et}{}_2Mo_2Co_2S_4(Cl)_2$ (**5**), respectively, in moderately high yields (68% (**4**) and 48% (**5**)) subsequent to crystallization from CH_2Cl_2/hexane. As observed with **3**, clusters **4** and **5** displayed ^{1}H NMR spectra typical of diamagnetic compounds and showed equivalent Cp^{Et} ligands on the clusters. Plots of δ_{Me} for the two Me signals *vs* the Allred−Rochow electronegativities of the halogens were linear and parallel with slopes of -0.33 ± 0.01 ($\Delta\delta/\Delta\chi$). The chemical shifts of the ethyl group varied only slightly and were not proportional to the electronegativities of the halogens. The far-IR spectrum for **4** showed a prominent band at 398 cm^{-1}, which is consistent with the (μ_3-S)−M stretching absorption, and Co−Br stretching frequencies at 250 and 293 cm^{-1}. The solid-state structure of **5** was determined by single-crystal X-ray diffraction and is presented below.

Cluster **2** also reacted with 1 equiv of PhSSPh in refluxing toluene to give, after 1 h, the analytically pure cluster $Cp^{Et}{}_2Mo_2Co_2S_4(SPh)_2$ (**6**) in 58% yield subsequent to crystallization from toluene/hexane at −18 °C. Alternatively, cluster **6** was prepared by the reaction of **1** with PhSH in refluxing toluene for 2.5 h. Recrystallization from toluene/hexane afforded crystals of **6** in only 17% yield, however. Unlike the ^{1}H NMR spectra obtained for clusters **3**−**5**, a ^{1}H NMR spectrum could not be recorded for **6**, presumably due to its paramagnetism. The far-IR spectrum of **6** showed prominent overlapping bands at 379 and 397 cm^{-1}, also consistent with (μ_3-S)−M stretching vibrations. The solid-state structure of cluster **6**, which was determined by single-crystal X-ray diffraction and communicated previously,[8] is discussed further in the present context (see below).

Structures of the $Cp^{Et}{}_2Mo_2Co_2S_4(X)_2$ (X = I, Cl, SPh) Clusters. Figures 1−3 show ORTEP plots of the structure of **3**, **5**, and **6**, respectively, with their atom numbering schemes. Selected interatomic distances and angles are collected in Table 1. Some other 58-VSE and 62-VSE clusters are listed in Table 2, and important interatomic distances are given for comparison with the clusters prepared in this work. Cluster **1** is a 60-VSE, electron-precise cluster which consists of a completely bound tetrahedral arrangement of metal atoms with six M−M bonds, imbedded within a tetrahedral array of S atoms. Clusters **3** and **5** are isomorphous and possess

(10) Sheldrick, G. M. *SHELXL PLUS*, v. 3.43/v; Siemens Analytical X-ray Systems, Inc.: Madison, WI, 1988.
(11) Sheldrick, G. M. *SHELXL-93. Program for crystal structure refinement*: University of Göttingen: Göttingen, Germany, 1993.
(12) Demadis, K. D.; Coucouvanis, D. *Inorg. Chem.* **1995**, *34*, 436.
(13) Nakamoto, K. *Infrared and Raman Spectra of Inorganic and Coordination Compounds*; Wiley-Interscience: New York, 1986.

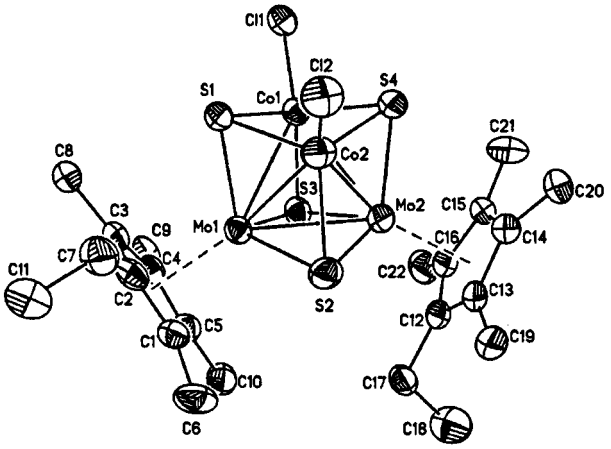

Figure 2. ORTEP plot of $Cp^{Et}{}_2Mo_2Co_2S_4(Cl)_2$ (**5**) with the atomic numbering scheme. Thermal ellipsoids are drawn at the 50% probability level.

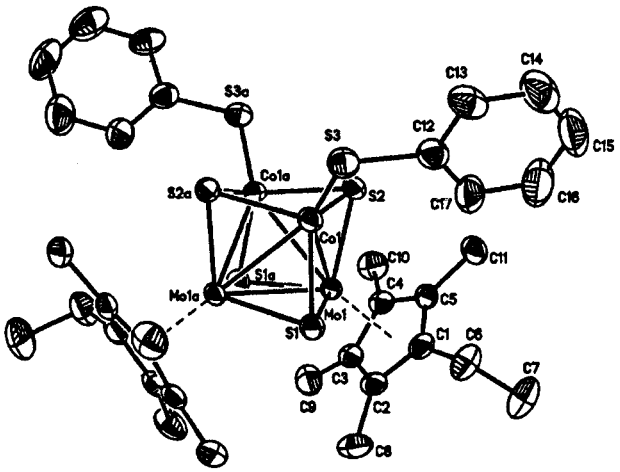

Figure 3. ORTEP plot of $Cp^{Et}{}_2Mo_2Co_2S_4(SPh)_2$ (**6**) with the atomic numbering scheme. Thermal ellipsoids are drawn at the 50% probability level.

Table 1. Selected Interatomic Distances (Å) and Angles (deg) for Clusters 1, 3, 5, and 6[a]

atoms	1[b]	3	5	6
		Distances		
Mo−Mo	2.8313(5)	2.803(1)	2.804(1)	2.8156(3)
Co−Co	2.5816(9)	2.936(1)	2.955(2)	2.7414(6)
av Mo−Co	2.6931(7)	2.738(4)	2.756(5)	2.733(1)
av Mo−S	2.324(3)	2.32(2)	2.31(2)	2.319(2)
av Co−S	2.20(2)	2.24(2)	2.25(2)	2.23(3)
		Angles		
av Mo−S−Mo	75.1(1)	73.94(6)	74.0(2)	74.26(1)
av Mo−S−Co	73.2(4)	74.1(1)	74.6(3)	73.8(1)
av Co−S−Co	71.34(2)	81.25(6)	81.2(1)	74.61(3)

[a] Standard deviations are given in parentheses. [b] Reference 14.

similar structural features. On going from **1** to **3** or **5**, the most striking structural consequence is the elongation of the Co···Co distance. The Co···Co distances in **3** and **5** are 2.936(1) and 2.955(2) Å, respectively, and are well beyond the typical Co−Co single bond distance which is observed in **1** (2.571(3) Å).[14] Thus, the substitution of CO in **1** with halogen in **3** and **5** results in the cleavage of a Co−Co single bond.

Clusters **3** and **5** are electron-deficient, 58-VSE clusters with five metal−metal bonds (which are expected to have 62 VSE if they are electron precise[15]). These clusters consist of a "butterfly" arrangement of metal atoms in the cluster core. Co atoms occupy the wingtip positions, and Mo atoms are at the hinge positions. The hinge angle between the two Mo_2Co triangular faces is 77.0° (**3**) or 77.3° (**5**) compared to 64.6° for **1**.[14] The Mo−Mo distances are the same in **3** and **5**, within experimental error. The (μ_3-S)−Co distances are slightly shorter than the (μ_3-S)−Mo distances and all are consistent with normal M−S single bond distances. None of the S atoms is bound to another S atom in these structures. Thus, aside from the dramatic increase in Co···Co distance, the core structure is minimally affected.

Cluster **6** maintains structural features similar to **1**, **3**, and **5**, although the Co···Co distance has an intermediate distance of 2.741(6) Å. This exceeds the distance expected for a conventional Co−Co single bond and is nearly identical to the Co···Co distance in the monoanion of $Cp'_2Mo_2Co_2S_4(CO)_2$, in which the Co···Co distance of 2.735(1) Å was associated with a Co···Co bond order of $^1/_2$, consistent with its 61 VSE count.[16] The electron count for **6**, 58 VSE, is the same as that in **3** and corresponds to an electron-deficient cluster with five M−M bonds. The four metal atoms in this cluster also form a butterfly arrangement of atoms imbedded within a tetrahedral array of unbound S atoms. The hinge angle between the two Mo_2Co triangular faces is 71.7°, a value which is also intermediate between that for **1** and those for **3** and **5**. Each S atom is triply bridging and caps a closed Mo_2Co face or open Co_2Mo face in the cluster core. The (μ_3-S)−Co and (μ_3-S)−Mo distances also correspond favorably with values expected for single bonds. It is also noteworthy that there is an increase in the Co−S−Co angle concomitant with the increase in the Co···Co intermetallic distance on going from **1** to **6**, **3**, and **5**.

Bonding in the Oxidized Cubane Clusters. The clusters **3**, **5**, and **6** are characterized by the general formula $Cp^{Et}{}_2Mo_2Co_2S_4(X)_2$, where X = I, Cl, and SPh, all one-electron donor ligands. A qualitative molecular orbital (MO) scheme for $M_2M'_2S_4$ clusters, where M is a 4d metal with a pseudooctahedral coordination sphere and M′ is a 3d metal with a pseudotetrahedral coordination sphere, has been developed by Harris.[17] In this model, the MOs for the metal-based cluster orbitals consist of 10 orbitals, 4 of which are low-lying, nonbonding MOs and 6 of which are higher energy, bonding MOs. The low-lying, nonbonding MOs are predominately M′ in character and result from stabilization of the e set of orbitals by π-acceptor ligands. Thus, the $[M_2M'_2]^{n+}$ core must supply 20 electrons to form a completely bound tetrahedron of metal atoms with 6 metal−metal bonds. The strongest metal−metal interactions in these clusters occur between the two 4d metals, and the weakest interactions are between the two 3d metals. For clusters **3**, **5**, and **6**, when we count the metal oxidation states as Co(III) and Mo(III), each Co contributes 6 electrons and each Mo contributes 3 electrons to the cluster core, giving a total of 18 electrons available to occupy the metal-based cluster orbitals for two Co atoms and two Mo atoms in each cluster. Of

(14) Curtis, M. D.; Riaz, U.; Curnow, O. J.; Kampf, J. W.; Rheingold, A. L.; Haggerty, B. S. *Organometallics* **1995**, *14*, 5337.

(15) Lauher, J. W. *J. Am. Chem. Soc.* **1978**, *100*, 5305.

(16) Curtis, M. D.; Druker, S. H.; Goosen, L.; Kampf, J. W. *Organometallics* **1997**, *16*, 231.

(17) Harris, S. *Polyhedron* **1989**, *8*, 2843.

Table 2. Selected Intermetallic Distances (Å) for Some 58 VSE Electron Deficient and 62 VSE Thiocubane Clusters

cluster	VSE	M′−M′ [a]	M−M′ [b,c]	M−M [d]	ref
$Cp'_2Mo_2Co_2S_4(CO)_2$ (**1**)	60	2.5816(9)	2.6931(7)	2.8313(5)	14
$Cp^{Et}_2Mo_2Co_2S_4(I)_2$ (**3**)	58	2.936(1)	2.738(4)	2.803(1)	*d*
$Cp^{Et}_2Mo_2Co_2S_4(Cl)_2$ (**5**)	58	2.955(2)	2.756(5)	2.8040(13)	*d*
$Cp^{Et}_2Mo_2Co_2S_4(SPh)_2$ (**6**)	58	2.7414(6)	2.7326(12)	2.8156(3)	*d*
$Cp'_2V_2Fe_2S_4(NO)_2$	58	2.590(1)	2.745(5)	2.957 (1)	18
$Mo_2Cu_2S_4(edt)_2(PPh_3)_2$	58	3.095(2)	2.810(20)	2.858(1)	19
$W_2Cu_2S_4(edt)_2(PPh_3)_2$	58	no bond	2.823(20)	2.851(1)	20
$[V_2Cu_2S_4(OC_4H_8dtc)_2(SPh)_2]^{2-}$	58	3.338(3)	2.781(10)	2.784(4)	21
$[V_2Cu_2S_4(Me_2dtc)_2(SPh)_2]^{2-}$	58	3.351(5)	2.777(15)	2.803(5)	22
$Cp'_2Mo_2Ni_2S_4(CO)_2$	62	2.962(2)	2.722(2)	2.829(1)	23a
$Cp'_2V_2Ni_2S_4(NO)_2$	62	3.022(1)	2.80(1)	2.871(1)	23b
$Cp^{Et}_2Mo_2Co_2S_4(NO)_2$	62	3.116(1)	2.764(4)	2.814(1)	24
$Cp^*_2W_2Co_2S_4(NO)_2$	62	3.131(1)	2.780(4)	2.798(1)	24

[a] M′ = Fe, Co, Ni, Cu. [b] M = V, Mo, W. [c] Average bond distance is listed, and standard deviations from the mean are in parentheses. [d] This work.

Table 3. Summary of Crystallographic Data for 3 and 5

	3	**5**
empirical formula	$C_{22.5}H_{35}S_4ClCo_2Mo_2I_2$	$C_{22}H_{34}S_4Cl_2Co_2Mo_2{\cdot}CH_2Cl_2$
fw	1032.80	892.37
cryst color and habit	black rectangular plate	black rectangular plates
cryst dimens (mm)	0.08 × 0.59 × 0.29	0.12 × 0.22 × 0.26
cryst syst	monoclinic	monoclinic
space group	*C*2/*c* (15)	*C*2/*c* (15)
a	39.540(7) Å	37.89(1) Å
b	10.737(2) Å	10.182(3) Å
c	16.485(2) Å	16.394(5) Å
β	106.95(1)°	107.92(2)°
volume	6694(2) Å^3	6016(3) Å^3
Z	8	8
density (calcd)	2.049 g cm^{-3}	1.97 g cm^{-3}
F(000)	3960	3552
linear abs coeff (*μ*)	38.51 cm^{-1}	25.21 cm^{-1}
scan type	*θ*/2*θ* scan	*θ*/2*θ* scan
2*θ* scan range	5−55°	5−52°
octants used	+*h*, +*k*, ±*l* (*h* 0/52; *k* 0/14; *l* 22/22)	±*h*, +*k*, +*l* (*h* −5−1/51; *k* 0/14; *l* 0/23)
scan rate	3−8°/min, variable	3.5−9.0°/min, variable
scan width	0.8° below $K_{\alpha1}$ to 0.8° above $K_{\alpha2}$	0.9° below $K_{\alpha1}$ to 0.9° above $K_{\alpha2}$
background/scan ratio	0.5	0.5
no. of data collected	8466	7357
no. of unique reflns	7122, R_{int} = 0.0165	6436, R_{int} = 0.000
relative max/min transmission	0.808/0.388	7.775/0.050
data/parameter ratio	18.8	20.2
R, R_w	0.0563, 0.0639[a]	0.0904, 0.2503[b]
GOF	1.41	1.065
mean shift/error	<0.001	<0.001
max shift/error	0.001	0.003
secondary extinction:	7.25(1) × 10^{-7}	0.00043(14)
residual electron density	+1.18/−0.87 e/Å^3	+1.98/−2.35 e/Å^3

[a] $R = \Sigma|\Delta F|/\Sigma|F_o|$ where $\Delta F = F_o - F_c$, and $R_w = \{\Sigma w|\Delta F|^2/\Sigma|F_o|^2\}^{1/2}$. [b] *R* as above, $R_w = \{\Sigma w|F_o^2 - F_c^2|^2/\Sigma|F_o^2|^2\}^{1/2}$.

the 18 electrons, 8 will fill the low-lying nonbonding orbitals leaving 10 electrons to fill 5 metal−metal bonding orbitals. Depending on the nature of these MOs, two extreme consequences are possible. If the MOs are highly delocalized over the entire $M_2M'_2$ core, the electron deficiency will be spread over all the bonds and the metal−metal distances might increase only slightly (bond orders of $^5/_6$). On the other hand, if the MOs are localized, then the electron density may be removed from just one metal−metal pair, leading to a butterfly arrangement of five M−M bonding distances and one M···M nonbonding distance. In between these extremes partial localization may result in elongation of one bond and slight spreading of the remaining M−M distances.

In the halo clusters **3** and **5**, it appears that the electron density has been removed from the Co−Co bond, resulting in a Co···Co nonbonding distance. In the thiolato cluster **6**, it appears that the electron density is preferentially, but not completely, removed from the Co−Co bond and an apparent bond order near 0.5 results. The electronegativity and/or *π*-donor characteristics of the ligands on the Co atoms evidently affect the degree of localization/delocalization of the cluster core MOs involved in Co−Co bonding.

Other examples of "$M_2M'_2S_4$" 58-VSE electron-deficient clusters and 62-VSE electron-precise clusters are listed in Table 2, where their intermetallic distances are compared. The butterfly arrangement observed in **3**, **5**, and **6** is also observed in these $M_2M'_2S_4$ clusters,[18−22] and the M−M, M−M′, and M−S (M = V, Mo, W; M′ =

(18) Rauchfuss, T. B.; Weatherill, T. D.; Wilson, S. R.; Zebrowski, J. P. *J. Am. Chem. Soc.* **1983**, *105*, 6508.
(19) Nianyong, Z.; Yitan, Z.; Xintao, W. *J. Chem. Soc., Chem. Commun.* **1990**, 780.
(20) Nianyong, Z.; Richu, W.; Xintao, W. *Acta. Crystallogr.* **1991**, *C47*, 1537.
(21) Liu, Q.; Yang, Y.; Huang, L.; Wu, D.; Kang, B.; Chen, C.; Deng, Y.; Lu, J. *Inorg. Chem.* **1995**, *34*, 1884.

Table 4. Crystallographic Data for $Cp^{Et}_2Mo_2Co_2S_4(SPh)_2$ (6)

empirical formula	$C_{34}H_{44}S_6Co_2Mo_2$
fw	954.836
cryst color and habit	black, irregular, plate-like
cryst dimens (mm)	0.62 × 0.08 × 0.20
cryst syst	monoclinic
space group	*C*2/*c* (15)
a	21.477(5) Å
b	9.478(2) Å
c	18.426(3) Å
b	90.95(2)°
volume	3750(1) Å^3
Z	4
density (calc)	1.69 g cm^{-3}
F(000)	1928
linear abs coeff (μ)	18.53 cm^{-1}
scan type	$\theta/2\theta$ scan
2θ scan range	5−55°
octants used	$+h, +k, \pm l$ (h 0/24; k 0/13; l 24/24)
scan rate	3−6°/min, variable
scan width	0.8° below $K_{\alpha1}$ to 0.8° above $K_{\alpha2}$
background/scan ratio	0.5
no. of data collected	6171
no. of unique reflns	4072, R_{int} = 0.0170
max/min transmission	0.862/0.626
data/parameter ratio	17.4
refined reflns with (F_o) ≥ 3σ(F)	3489
R, R_w	0.0329, 0.0388
GOF	1.25
mean shift/error	<0.001
max shift/error	0.001
secondary extinction	5.14(2) × 10^{-7}
residual electron density	+0.71/−0.47 e/Å^3

Fe, Co, Ni, Cu) distances correspond to single bonds. The M′−M′ distances are nonbonding except in the 60-VSE cluster, as expected. (The sole exception to these generalizations occurs in the compound $Cp'_2V_2Fe_2S_4(NO)_2$, wherein it is the V−V distance that is nonbonding while the Fe−Fe distance is bonding. Apparently, in this compound the roles of the early and late transition metals are reversed.) In contrast to the bonding pattern in Table 2, however, the 58-VSE cluster, $Cp_3Mo_3FeS_4(SH)$ possesses a C_{3v} symmetric M_3M' tetrahedron and *all* metal−metal contacts are bonding.[13] Thus, the electron deficiency appears to reside in a weakly metal−metal bonding, highly delocalized MO in $Cp_3Mo_3FeS_4(SH)$. The nonbonding distances observed in the 58-VSE clusters also compare quite favorably with the nonbonding distances in several 62-VSE thiocubane clusters, *e.g.*, $Cp_2Mo_2Ni_2S_4(CO)_2$[23a] and $Cp_2V_2Ni_2S_4(NO)_2$.[23b] In the 62-VSE clusters, the structural data suggest that two electrons occupy a M′−M′ antibonding orbital, imparting a M′−M′ bond order of zero.

Magnetism in the Oxidized Cubane Clusters. The magnetic susceptibilities of the clusters **3**, **4**, **5**, and **6** were measured on a SQUID magnetometer. On the basis of the ^{1}H NMR spectroscopy, cluster **6** behaved as expected and exhibited paramagnetic behavior. A plot of $1/\chi_{corr}$ *vs T* (Figure 4) is a straight line, the slope of which gives an effective magnetic moment of 3.49 μ_B, a value in the range observed for $S = 1$ spin systems.[25] An EPR spectrum for **6** could not be recorded, consistent with the assignment of an integer spin state.

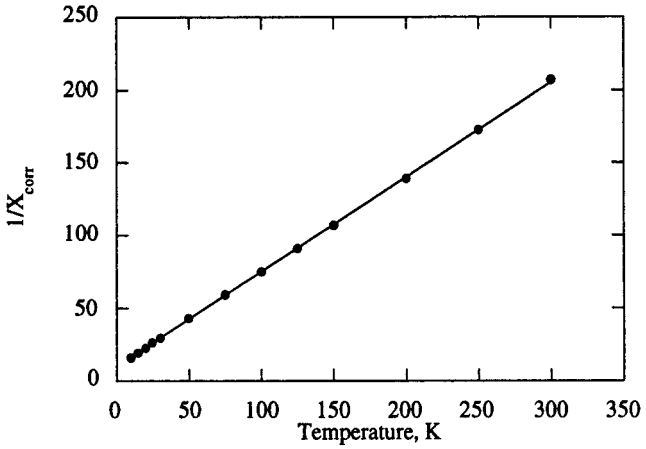

Figure 4. Plot of $1/\chi_{corr}$ *vs T* for $Cp^{Et}_2Mo_2Co_2S_4(SPh)_2$ (**6**). The points are experimental values; the solid line is the linear curve fit.

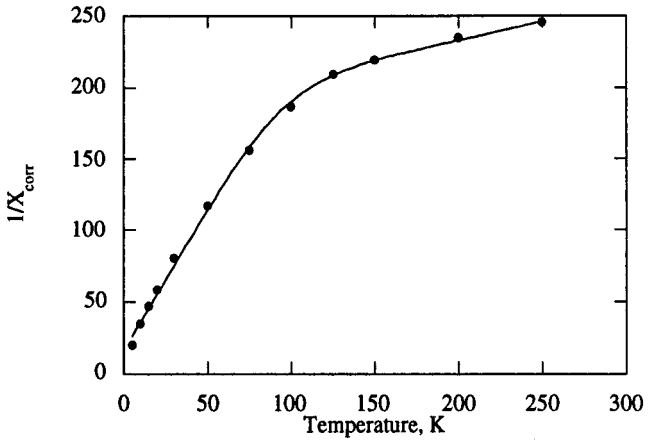

Figure 5. Plot of $1/\chi_{corr}$ *vs T* for $Cp^{Et}_2Mo_2Co_2S_4(Br)_2$ (**4**). The points are experimental values; the solid line was calculated as described in the text.

As previously indicated, the ^{1}H NMR spectra for clusters **3**, **4**, and **5** showed clean patterns corresponding to those expected for the Cp^{Et} ligands on diamagnetic clusters. For **3**, no shift, but a slight broadening, was seen in the proton resonances at lower temperatures (to −40 °C). Contrary to expectations based on their NMR behavior, however, clusters **3**, **4**, and **5** also were paramagnetic. Plots of $1/\chi_{corr}$ *vs T* for **3**,[8] **4** (Figure 5), and **5** (Figure 6) were not linear. The observed deviation from linearity in these plots is consistent with the occupation of one or more excited states of higher spin multiplicity. Accordingly, the data for each cluster were fitted with the Van Vleck equation.[26] For cluster **3**, the best fit between the calculated and observed values was obtained for a model with a triplet ground state and $S = 2$ and 3 levels at $\Delta E_1 = 203$ cm^{-1} and $\Delta E_2 = 686$ cm^{-1}, respectively, above the ground state. Corresponding to these values, the occupations of the excited $S = 2$ and 3 levels are 37.5% and 3.7%, respectively, at room temperature. From the calculated expression, the derived values for μ_{eff} are $\mu_1 = 2.98$ μ_B and $\mu_2 = 4.79$ μ_B. These values compare favorably with the theoretical μ_{eff} (spin-only) for $S = 1$ ($\mu_{eff} = 2.83$ μ_B) and $S = 2$ ($\mu_{eff} = 4.90$ μ_B) spin systems. An analogous approach to that

(22) Yang, Y.; Liu, Q. *Acta. Crystallogr.* **1993**, *C49*, 1623.
(23) (a) Curtis, M. D.; Williams, P. D.; Butler, W. M. *Inorg. Chem.* **1988**, *27*, 2853. (b) Rauchfuss, T. B.; Gammon, S. D.; Weatherill, T. D.; Wilson, S. R. *New J. Chem.* **1988**, *12*, 373.
(24) Mansour, M. A.; Curtis, M. D.; Kampf, J. W. *Organometallics* **1997**, *16*, 275.
(25) Drago, R. S. *Physical Methods in Chemistry*; Saunders College Publishing: Chicago, IL, 1977.

(26) The form of the Van Vleck equation used was $1/\chi_m(T) = (\sum_i(2S_i + 1)\cdot\exp(-\Delta E_i/kT))/(\sum_i(2S_i + 1)\chi^i\cdot\exp(-\Delta E_i/kT)) + X$, where $\chi_i = (N\mu_i^2\beta^2)/(3kT)$. The symbols have their usual meanings.

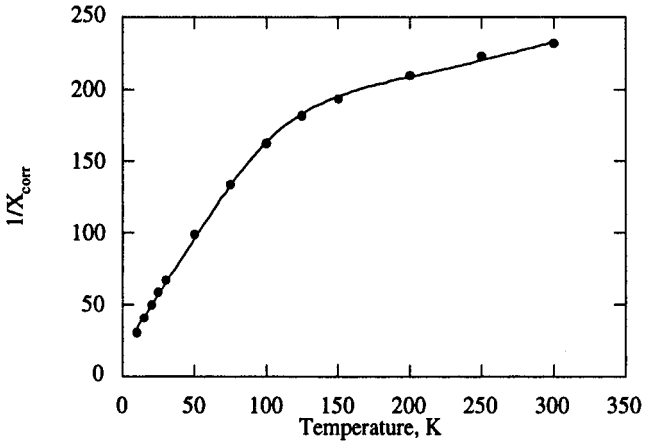

Figure 6. Plot of $1/\chi_{corr}$ *vs* T for $Cp^{Et}{}_2Mo_2Co_2S_4(Cl)_2$ (**5**). The points are experimental values; the solid line was calculated as described in the text.

used in the fitting routine for the data for **3** was used for the data for **4** and **5**. The final best fit for $1/\chi_{corr}$ *vs* T for **4** revealed that $\Delta E_1 = 283$ cm^{-1} and $\Delta E_2 = 1140$ cm^{-1}. Analogous to the magnetic data observed for **3**, these values correspond to a triplet ground state, and the occupation of the excited $S = 2$ and 3 levels are 25.5% and 0.4% at room temperature. From the calculated expression, the derived values for μ_{eff} are $\mu_1 = 2.03\ \mu_B$ and $\mu_2 = 4.73\ \mu_B$. The final best fit for $1/\chi_{corr}$ *vs* T for **5** also gave a triplet ground state and $S = 2$ and 3 levels at $\Delta E_1 = 319$ cm^{-1} and $\Delta E_2 = 1655$ cm^{-1}, respectively. The latter are occupied to the extent of 21.4% and 0.03% at room temperature. From the calculated expression, the derived values for μ_{eff} are $\mu_1 = 2.27\ \mu_B$ and $\mu_2 = 5.28\ \mu_B$. On the basis of the very small contribution of the third term in the expression for **5**, it might appear that it is not needed to accurately fit the observed data. However, when the $S = 3$ term was excluded from the expression, the theoretical fit deviated significantly from the experimental values for $1/\chi_{corr}$ at temperatures above 200 K.

In the halide-substituted clusters, **3**, **4**, and **5**, the energies to access the higher spin states increase as the π-donor ability of the halide increases (Cl > Br > I). Thus, the simple paramagnetism observed for cluster **6** may simply mean that the $S = 2$ state is not thermally accessible at the temperatures studied, since thiolate ligands are better π-donors than the halide ligands.

The diamagnetic-appearing ^{1}H NMR spectra for clusters **3**, **4**, and **5** suggested that these clusters might exhibit different magnetic behavior in solution than in the solid state. The effective moments obtained for **3**, **4**, **5**, and **6** in solution[27] at room temperature were $\mu_{eff} = 3.24$, 2.52, 1.84, and 2.36 μ_B, respectively. These values are all lower than the corresponding solid state values of $\mu_{eff} = 3.92$, 3.03, 3.22, and 3.40 for **3**, **4**, **5**, and **6**. The magnetic behavior in these clusters may be related to the M′−M′ separation. It has been shown that metal−metal bonds in metal−sulfur clusters may

Scheme 2

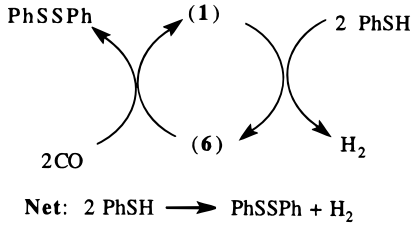

be mobile in solution,[28] so variations in metal−metal bond distances in response to solvation may account for the observed differences in the solution and solid state magnetic data. In any event, these data show that the halo clusters are paramagnetic in solution as well as in the solid state, leaving us with no apparent explanation for their diamagnetic-appearing ^{1}H NMR spectra.

Reactivity of the Oxidized Cubane Clusters. We were especially interested in determining whether or not these oxidized cubane clusters could be reduced back to the starting carbonyl cluster **1**. If so, then a *catalytic* desulfurization cycle might be possible. Accordingly, a solution of **6** in toluene was allowed to react with H_2 (200 psi)/CO (200 psi) at 130 °C for 10 h. A solution IR spectrum of the product mixture revealed $\nu_{CO} = 1956$ and 1973 cm^{-1}, corresponding to the CO absorptions for **1** in toluene. The solvent was removed from the reaction mixture, and the residual solid was extracted with hexane. A GC-MS analysis of the extract revealed the presence of PhSSPh ($M^+ = 218$) as the sole organic product. Thus, the reaction proceeded according to eq 1. Since cluster **1** reacted with PhSH to form **6** and **6**

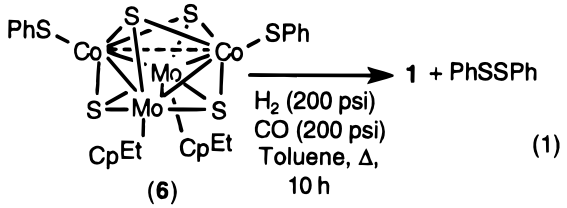

(1)

reacted with CO to regenerate **1** and form PhSSPh, the catalytic cycle for the conversion of PhSH into PhSSPh and H_2 according to Scheme 2 seemed possible. Thus, **1** was allowed to react with a large excess (162 equiv) of PhSH under CO (1000 psi) at 150 °C for 46 h. Cluster **6** was obtained as the organometallic product in an isolated yield of 56% (based on **1**), and PhSSPh (171%) and PhS(CO)Ph (161%) were obtained as the organic products. Some insoluble, black solid, presumably consisting primarily of the putative sulfide-bridged poly(cubane) (**2**), was also obtained and removed from the product mixture by filtration through Celite. As expected, therefore, the formation of PhSSPh occurred, and the catalytic cycle shown in Scheme 2 was effected. The phenylthiobenzoate product was unexpected, but it must arise from the catalytic desulfurization of PhSH. A plausible reaction sequence for its formation is shown in Scheme 3.

The phenylthiobenzoate product suggested that metal−carbon (Co−Ph) bonds (intermediate **7**) were formed during the desulfurization reaction, followed by insertion of CO into the metal−phenyl bond to give an acyl

(27) The Evan's method for magnetic susceptibility was utilized. The formula for superconducting NMR spectrometers is $\chi_g = (-3\Delta f)/4\pi fm + \chi_o(d_o - d_s)/m$ where χ_g = mass suceptibility of the solute (cm^3/g); Δf = observed frequency shift of reference resonance (Hz); f = spectrometer frequency; χ_o = mass susceptibility of solvent (cm^3/g); m = mass of substance per cm^3 of solution; d_o = density of solvent (g/cm^3); and d_s = density of solution, see: Schubert, E. M. *J. Chem. Educ.* **1992**, *69*, 62. The original description of the method can be found in Evans, D. F. *J. Chem. Soc.* **1959**, 2003

(28) Venturelli, A.; Rauchfuss, T. B. *J. Am. Chem. Soc.* **1994**, *116*, 4824.

Scheme 3

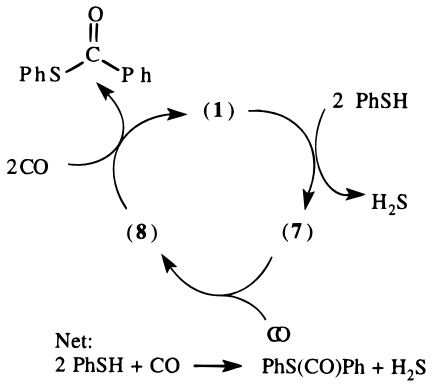

intermediate (**8**). The acyl intermediate could then react with the excess PhSH and/or CO present to split out phenylthiobenzoate. (A referee suggested a complimentary pathway: CO insertion into the Co−SPh bond, followed by reductive elimination of PhCOSPh.) These proposed pathways lack any mechanistic detail. An alternative pathway for the formation of benzoyl group is the homolysis of the C−S bond to produce the phenyl radical,[7] followed by its reaction with CO to form the benzoyl radical. However, H atom transfer from PhSH to the radicals with the formation of benzene or benzaldehyde should be rapid, but no PhCHO was detected in the product mixture.

One test of the proposal for the formation of metal−aryl-bonded intermediates in the catalytic reaction shown in Scheme 3 is their independent syntheses. Therefore, we sought to prepare an alkyl or aryl derivative of the oxidized clusters by nucleophilic substitution of halide with RLi, RMgBr, ZnR_2, or AlR_3 reagents. When **3** was allowed to react with PhLi, PhMgBr, EtMgBr, and MeLi, no reaction was observed either at room temperature or at reflux temperature in THF. Cluster **4** was allowed to react with PhLi in the hope that the less bulky bromo derivative would show enhanced reactivity. A reaction appeared to occur immediately as the solution color changed from deep green to dark brown upon addition of PhLi to the solution of **4**. The organometallic product could not be identified by ^{1}H NMR spectroscopy, and the elemental analysis did not correspond to any anticipated product, *e.g.*, substituted or reduced cluster.

Removal of solvent and extraction of the residual solid with hexane did reveal, however, the presence of biphenyl ($M^+ = 154$) by GCMS. Reduction of the cluster with PhLi and subsequent coupling of the phenyl radicals would give the observed organic product. Instability of a reduced cluster may account for the failure to obtain a tractable product. Alkyl nucleophiles which are milder reducing agents, *i.e.*, EtMgBr, $ZnEt_2$, $AlMe_3$, were used in analogous reactions. In none of these experiments could the fate of the organometallic product be determined. Thus, we were unable to model the formation of an intermediate with a Co−Ph bond as shown in Scheme 3. This failure does not, however, preclude this pathway as a possibility.

Conclusions

The halide- and thiolate-substituted clusters **3**, **4**, **5**, and **6** represent a new group of 58-VSE electron-deficient clusters which are prepared readily in good yields by the oxidative conversion of **1** with halogens, phenyl disulfide, or benzene thiol. The structural changes in the cluster core suggest that the formal two-electron oxidation removes electron density associated with the Co−Co σ-bond. We believe that these new, oxidized clusters are good models for the organometallic product that is formed in the desulfurization reaction of **1** with thiiranes and thietanes.[8] Furthermore, the partial regeneration of **1** from the proposed μ_2-S-bridged poly(cubane) (**2**) was modeled by the regeneration of **1** from **6**. These experiments lend support to the proposition that at least a portion of the organometallic product in the desufurization reactions consists of cubane clusters linked by μ_2-sulfide bridges. In a separate reaction, **1** was shown to facilitate the catalytic conversion of PhSH to PhSSPh and PhS(CO)Ph and **6** was the predominant organometallic product. Thus, the oxidized clusters may be desulfurization catalysts as well, but further work is necessary to identify the true nature of the catalytically active species.

Acknowledgment. The authors are grateful for the support furnished by the National Science Foundation, Grant Nos. CHE-9205018 and CHE-9523056.

Supporting Information Available: Tables of data collection parameters, bond lengths, bond angles, fractional atomic coordinates, anisotropic thermal parameters, and hydrogen atom fractional coordinates for **3**, **5**, and **6** and a plot of $1/\chi$ *vs T* for **3** (21 pages). Ordering information is given on any current masthead page.

OM9700932